

Fabrication of Mg-Zn/Al and Mg-Zn/Anodized Al Multilayered Composites by Accumulative Roll Bonding, Investigation of Corrosion Behavior

Ramesh Sampath¹ , Gajanan Anne^{2,*} , Gajanan Manjunath Naik¹ , Shamanth Vasanth³  Madhu Sudana Reddy⁴ 

¹ Department of Mechanical Engineering, RV Institute of Technology and Management, JP Nagar, Bengaluru, India – 560076; rameshs.rvitm@rvei.edu.in (R.S.); gajannaik@gmail.com (G.M.N.);

² Department of Mechanical Engineering, Shri Madhwa Vadiraja Institute of Technology and Management, Udupi, India – 574115; gajanan.mech@sode-edu.in (G.A.);

³ Department of Mechanical Engineering, REVA University, Bangalore, India - 560024; shamanth053@yahoo.co.in (S.);

⁴ Department of Mechanical Engineering, Oxford College of Engineering, Bangalore, India -560068; maddy_reddy@rocketmail.com (M.S.R.G.);

* Correspondence: gajanan.anne25@gmail.com (G.A.);

Scopus Author ID 57211503636

Received: 14.01.2022; Accepted: 15.02.2022; Published: 9.03.2022

Abstract: Mg-2%Zn/Al and anodized Mg-2%Zn/Al multilayered composites were developed from wrought Mg-2%Zn alloy with aluminum and anodized aluminum by accumulative roll bonding (ARB). The grain size was found to be 700-750 nm and the lowest density of 2122 kg/m³ after roll bonding. The corrosion behavior of the multilayered composites has been examined using electrochemical polarization, zero resistance ammeter, and hydrogen evolution tests. Low corrosion current density, high induction time to passive film breakdown, and low hydrogen evolution are the significant features of multilayered Mg-2%Zn/Al and anodized Mg-2%Zn/Al composites. This feature is because of grain refinement, formation of additional β phases ($Al_{12}Mg_{17}$ and $AlMg_4Zn_{11}$), and presence of Al_2O_3 .

Keywords: magnesium; accumulative roll bonding; ultrafine grain; multilayered composites; corrosion.

© 2022 by the authors. This article is an open-access article distributed under the terms and conditions of the Creative Commons Attribution (CC BY) license (<https://creativecommons.org/licenses/by/4.0/>).

1. Introduction

Lightweight materials are the most demanding materials in aviation, transportation, electronics, and construction. They possess high strength and low weight, good damping capacity, thermal & electrical conductivity, and optimum corrosion resistance. Mg alloys are considered highly promising materials for lightweight applications [1-4]. However, the corrosion behavior of Mg alloy has been a major challenge due to the high electronegative potential of Mg metal which limits to use in many engineering applications [5]. Conventional methods used to enhance mechanical properties and corrosion behavior is either by an alloy design or severe plastic deformation (SPD) [6,7]. Accumulative roll bonding (ARB) is one of the SPD techniques to produce high strength as well as corrosion resistance by reducing the grain size. ARB is used to develop multilayered composites using similar and dissimilar materials with high productivity, low cost, and defect-free microstructure [8].

Corrosion behavior has been reported by many researchers, who have worked on various Mg alloys like AZ(Mg–Al–Zn), AM(Mg–Al–Mn), and ZK (Mg–Zn–Zr) series, and it

has been elucidated that corrosion resistance is directly affected by microstructures, surface finish and presence of secondary phases [9,10]. Nowadays, Mg-Zn alloys are the most widely used alloyed materials for a number of structural applications. Walter and Kannan [11] have found that corrosion current density and polarization resistance of AZ91 Mg alloy varied significantly with surface roughness. Aung and Zhou studied the effect of grain size of AZ31B on corrosion in the presence of 3.5 wt.% NaCl solution [12]. A significant corrosion rate reduction due to changes of grains from 250 to 65 μm was observed. Zhang *et al.* investigated AZ31 D Mg alloy for corrosion and the role of secondary phases (β phases) and its volume fractions on corrosion [13] and developed a relationship with corrosion current density and volume fractions of β phase.

In the present work, an effort was put to improve the corrosion behavior of Mg alloy by adopting alloy development, surface treatment (anodization), and bonding with Al through the accumulative roll bonding process. Paper deals with developing multilayered composites of wrought Mg-2%Zn alloy with Al and anodized Al using an accumulative roll bonding (ARB) process to examine the corrosion behavior of these newly developed newly developed multilayered composites using 0.1 M NaCl solution using potentiodynamic polarization, zero resistance ammeter, and hydrogen evolution tests.

2. Materials and Methods

2.1. Materials.

Binary alloys Mg-2%Zn and pure aluminum are used in the present study. Pure magnesium ingots and zinc granules are used to prepare Mg-2%Zn binary alloy by melting in the range of 750 - 800 $^{\circ}\text{C}$ under the inert atmosphere of 99% CO_2 in an electrical resistance furnace and with the help of mechanical agitation, segregation of alloying elements was controlled. After casting, Mg-2% Zn binary alloy was homogenized at 400 $^{\circ}\text{C}$ for 24 h. Then Mg-2%Zn alloy slabs with the dimensions of 40mm \times 30mm \times 10mm thick were cut from the cast ingot. The process was subjected to rolling with 0.25% reduction per pass at a rolling temperature of 300 $^{\circ}\text{C}$ with an intermediate heating time of 10 min. Finally, Mg-2%Zn binary alloy was rolled into 1 mm thick for accumulative roll bonding. Similarly, pure cast aluminum is also rolled to 1 mm thick by the same technique.

2.2. Anodization.

Before ARB process, Al sheet was cleaned using NaOH and HNO_3 and followed by anodization treatment using 15 wt % H_2SO_4 solution at 18 $^{\circ}\text{C}$ for 60 min at a voltage of 16 V. [14]. Anodization duration of one hour yields a uniform aluminum oxide film of about 10 μm , examined by scanning electron microscope (SEM).

2.3. ARB.

Figure 1 shows the ARB process, which involves four steps: surface preparation, stacking & furnace heating, rolling, and cutting for one complete cycle. Mg-2%Zn binary alloys and pure Al sheet were cleaned using acetone, wire-brushed, stacked together, and heated in the furnace for 10 min at 300 $^{\circ}\text{C}$. Rolling was carried out immediately, with a thickness reduction of 50% using a laboratory rolling mill (\varnothing 110 mm). The sheets are subjected to five ARB passes to obtain 32 layers (alternate) of Mg-2%Zn and Al. In the second material

system, anodized Al was roll bonded with the Mg-2%Zn to obtain 32 layered composites after sequentially performing five ARB passes. Sample codes for various processed conditions are tabulated in Table 1.

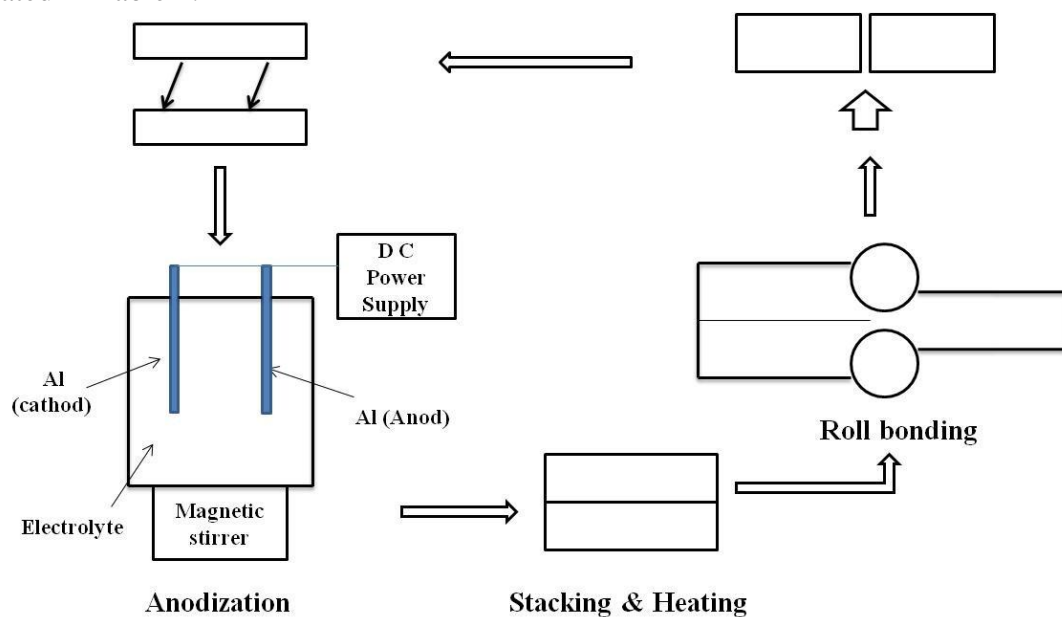


Figure 1. Schematic diagram of anodization and ARB process.

Table 1. Sample code.

S. No.	Processing condition	Sample code
1	Rolled Mg-2%Zn	R-1
2	Mg-2%Zn/Al multilayered composite	C-1
3	Anodized Mg-2%Zn/Al multilayered composite	AC-1

2.4. Characterization.

ARB processed samples were prepared for microstructural analysis using the following stages: polished using SiC paper and superfine diamond paste and etched with picral acetate solution. An optical microscope (OM) and Scanning Electron Microscope (SEM) were used to characterize the samples. Different phases in the roll bonded C-1 and AC-1 samples were identified by using X-ray diffraction (XRD) with Cu K α radiation.

2.5. Electrochemical measurements.

Electrochemical corrosion measurements like potentiodynamic polarization and zero resistance ammeter tests were performed at room temperature using EC lab-Biologic SP-150 with a scan rate of 1 mV/s. The electrode was immersed in an electrochemical cell containing 200 ml of 0.1 M NaCl of 7.5 pH. 0.1 cm² area of the sample was exposed to the electrolyte solution, and the distance between electrodes was maintained at 30 mm. The corrosion potential (E_{corr}) and corrosion current density (i_{corr}) were calculated by extrapolating Tafel plots. The surface morphology of the composite was examined after electrochemical corrosion tests with the help of SEM.

In the ZRA test, galvanic coupling current density and galvanic potential between two identical electrodes were measured simultaneously every 0.5 s for 120 min. In addition, induction time for the passive film to break down under open-circuit conditions was measured. ZRA test results were plotted up to the first passivity breakdown, which was observed as a sudden fall in the E_{corr} -ZRA values and an abrupt rise in the i_{corr} -ZRA values. In ZRA test, fluctuation in current in the electrodes was measured. Further, fluctuations in the potential

difference between the reference electrode (SCE) and working electrodes were recorded without external voltage. At the beginning of corrosion, a decrease in potential and increase in current density was observed in the working electrodes. Theoretically, there should be no net current flow between the electrodes. However, in practice, change in the environmental condition leads to currents flow and electrochemical noise, resulting in statistical variation in the corrosion rate across the surface. ZRA test was carried out three times for each sample, and good reproducibility was observed.

2.6. Immersion corrosion.

An immersion corrosion test was carried out according to ASTM G31-72. The hydrogen evolution during the immersion test is proportional to the corrosion rate of the materials. For the immersion study, multilayered composites were cut normal to the rolling direction and were finely polished. The hydrogen evolution test was carried out in 0.1 M NaCl solution for 120 h at room temperature. At the beginning of the immersion test, the pH was adjusted to 7.5, and hydrogen evolution and pH were recorded throughout the process. The corrosion rate was calculated using the following equations [15].

$$P_H = 3.65 \frac{\Delta w}{\rho} \quad (1)$$

where P_H = Corrosion rate through hydrogen evolution (mm/y)

ρ = Metal density (g/cm³)

Δw = Weight loss rate (mg/cm²/d)

$$\Delta w = 1.085 V_H \quad (2)$$

where V_H = Hydrogen evolution rate (ml/cm²/d)

3. Results and Discussion

3.1. Microstructure analysis.

Figure 2 shows the SEM image of the R-1 sample revealed bimodal grain size distribution with an average grain size of 6 μm and deformed twins. During the ARB process, the original grains are divided into many lamellae by twinning and dynamic recrystallization during the hot rolling process [16].

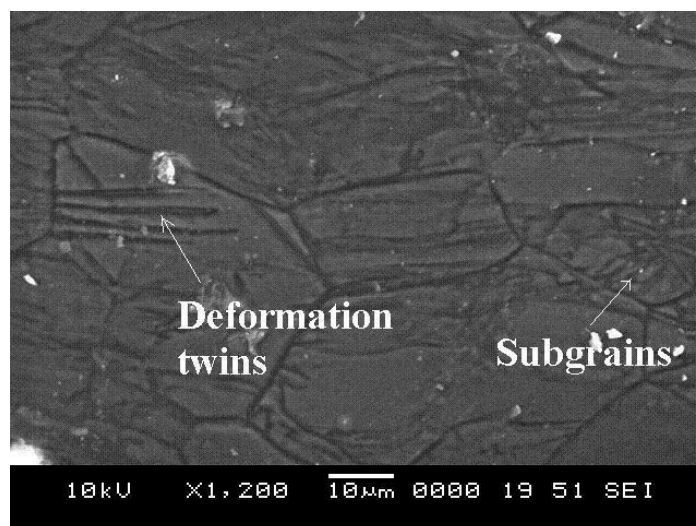


Figure 2. SEM micrographs of hot rolled Mg-2%Zn binary alloy.

3.2. ARB Microstructure.

Figure 3 shows the SEM micrographs of C-1 sample after five ARB passes. The average grain size in Mg-2%Zn and Al regions, after 5 ARB passes, was 750 nm and 700 nm, respectively (Figure 3c). Figure 3c shows alternate layers of thickness 35-40 μm of Al (region I) and Mg-2%Zn (region II) at the interface (region III). As the number of ARB passes increased, grain size reduced due to microstructure refinement because of dynamic recovery and recrystallization [17].

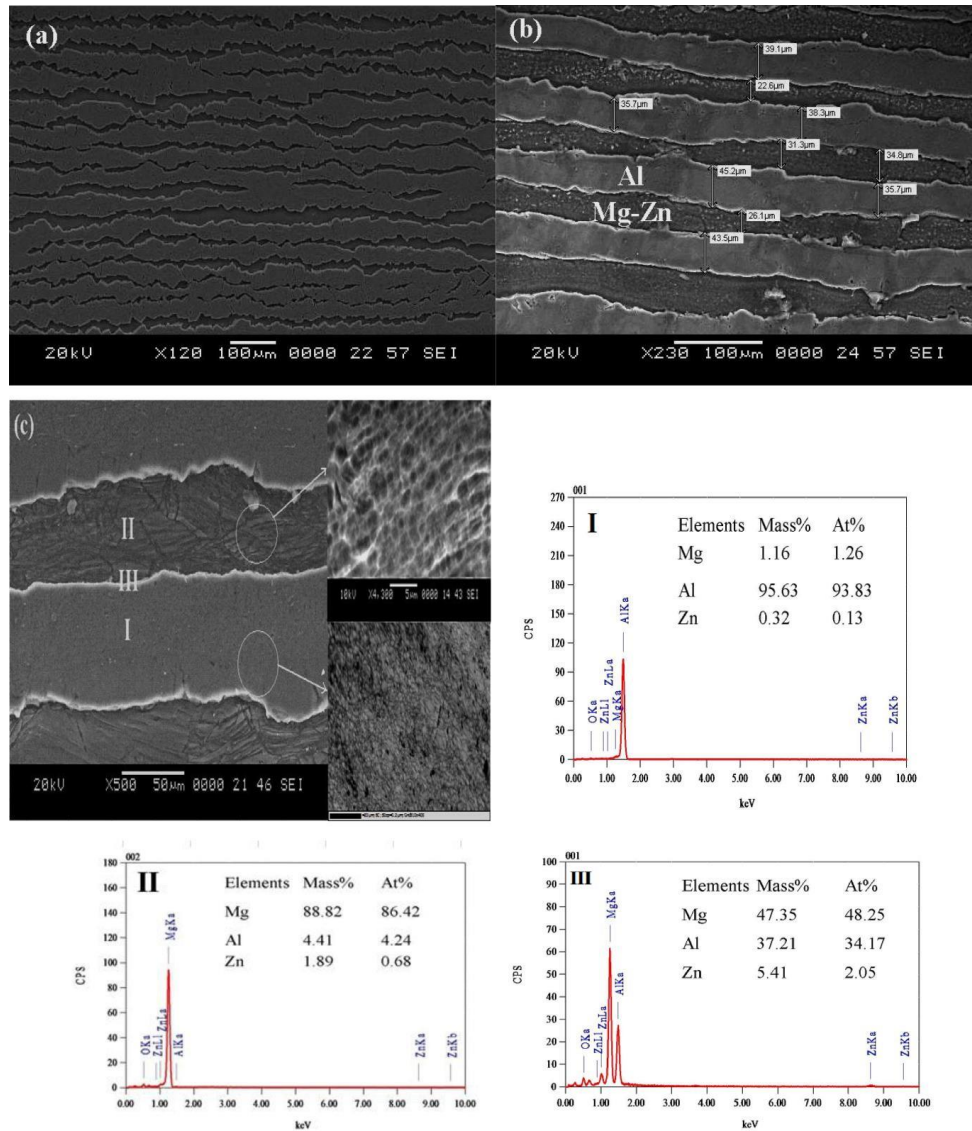


Figure 3. SEM micrographs of C-1 sample processed by ARB. (a) C-1 sample after five ARB passes; (b) enlarged image with measured thickness; (c) composition of the different layers and its interface by EDX analysis.

3.3. X-ray diffraction analysis.

XRD patterns of the C-1 and AC-1 (Figure 4) revealed the peaks indexed to Al, αMg , $\text{Al}_{17}\text{Mg}_{12}$, and $\text{AlMg}_4\text{Zn}_{11}$, as intermetallic phases, along with Al_2O_3 peaks. The formation of intermetallic phases revealed in multilayered composites maybe because of the grain boundary area, dislocation density, and high rolling strain induced into the material during ARB at 300 $^\circ\text{C}$, which increases the bonding of different layers in the multilayered composite [18,19].

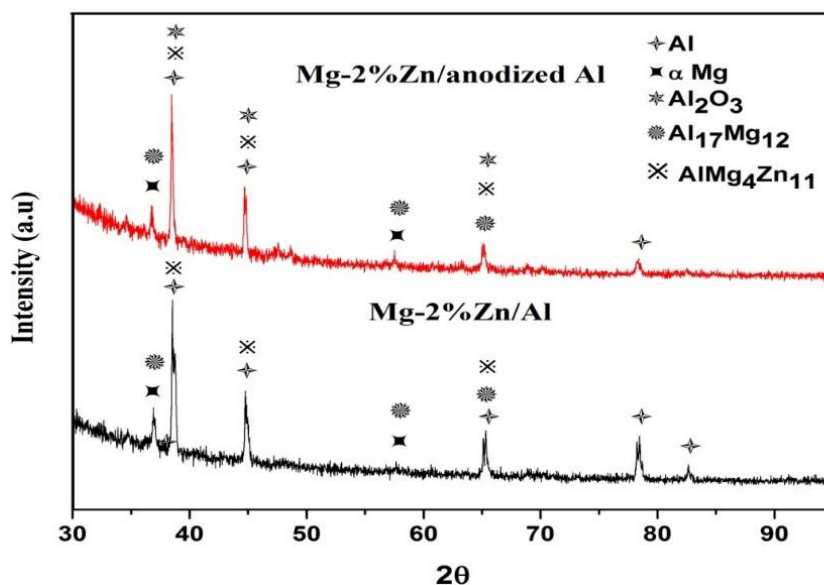


Figure 4. XRD patterns of the C-1 and AC-1 samples.

3.4. Potentiodynamic polarization studies.

Electrochemical corrosion plots of multilayered composites are shown in Figure 5, and electrochemical kinetics parameters are presented in Table 2. E_{corr} values of R-1, C-1 and AC-1 is -1.63, -1.40 and -1.36 VSCE, respectively. Shifting E_{corr} values towards the noble direction indicates lower corrosion current density (i_{corr}) exhibited because of the ARB process. R-1 sample exhibits high evolution of H_2 as compared to ARB processed composites due to cathodic reduction reactions. To examine the stable passivation behavior of alloy and composite in exposed environments, passive current density provides a better representation of uniform and localized corrosion. Reduction in passive current density was observed in roll bonded composites compared to the R-1 sample. The corrosion resistance of ultrafine-grained multilayered composites increased due to decreased cathodic kinetics, passivation kinetics [20], and formation $Al_{12}Mg_{17}$ and $AlMg_4Zn_{11}$ [21].

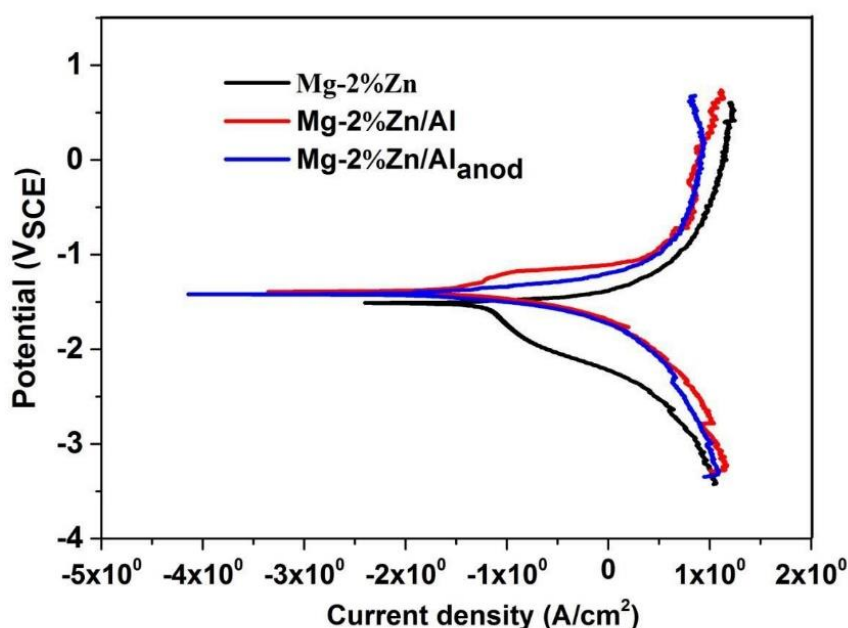


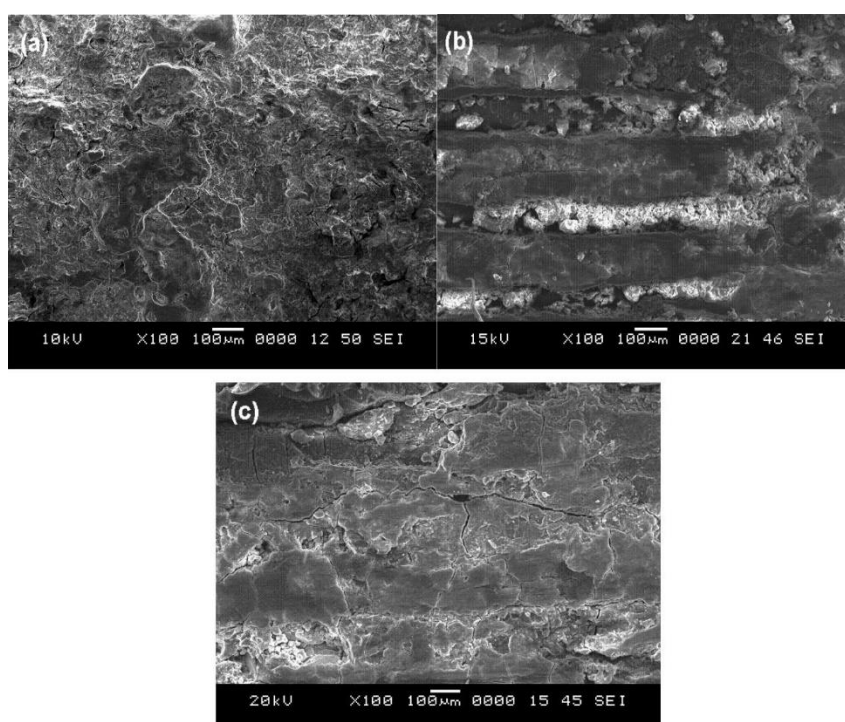
Figure 5. Potentiodynamic polarization curves of the R-1, C-1, and AC-1 samples.

Table 2. Electrochemical kinetic parameters.

Materials	E_{corr} (VSCE)	i_{corr} ($\mu\text{A}/\text{cm}^2$)	β_a (mV/decade)	β_c (mV/decade)	Corrosion rate (mm/y)
R-1	-1.63	77.96	238.1	- 882.2	2.38
C-1	-1.36	32.73	372.4	-180.8	1.69
AC-1	-1.40	30.14	119.2	-172.9	1.49

ARB has the advantage of breaking secondary phases with uniform distribution of ultrafine-grained microstructure. These intermetallic (β) phases act as an effective barrier and work as an active cathode concerning the active Mg matrix [22,23]. The corrosion resistance of the roll bonded AC-1 sample is high compared to C-1. The presence of rich Al_2O_3 on the surface of the anodized aluminum act as a barrier [24,25], a significant shift of E_{corr} in a noble direction, and lower i_{corr} values were noticed for the AC-1 sample. The i_{corr} value of AC-1 sample is 0.00465 times the value of C-1 sample. Hence, the corrosion resistance of ultrafine-grained AC-1 has significantly improved by anodization treatment, where aluminum oxide particles were introduced in the multilayered with the network of intermetallic phases.

Significant dissolution of the Mg-Zn alloy layer was observed (Figure 6 a-c). It has also depicted those corrosion products from dissolved alloy slightly covered the pure Al layer. However, the roll bonded composite sample did not show any dissolution because of the anodization of Al before the ARB process. A cracking tendency of the anodized layer was found due to the high hardness of the surface (alumina).

**Figure 6.** SEM micrographs of corroded (a) R-1; (b) C-1; (c) AC-1.

3.5. Zero Resistance Ammetry.

ZRA technique was used to represent the combined behavior of passivation and passivity break down with given time for Mg-Zn alloys and roll bonded composites in 0.1M NaCl for 5400 s (Figure 7). i_{corr} -ZRA was measured from the ZRA curves was found to be in the range of 1.29-0.77 mAcm^{-2} , and induction time to passivity breakdown increases from 1400, 1700, and 1800 s for the Mg-2%Zn alloy and roll bonded samples, respectively. It reveals that i_{corr} -ZRA decreases as the E_{corr} -ZRA increase with time. ZRA curves depict that higher

icorr-ZRA was observed in the R-1 sample as compared to C-1 and AC-1, which is also well justified with polarization curves (Figure 5).

The ZRA and polarization tests show a good agreement with their results, indicating that ARB processed multilayered composites show a reduction in corrosion current density was observed, and stability of passive film breakdown has been increased. Induction time to passive film breakdown gradually increased for C-1 and AC-1 samples compared to R-1, clearly indicated in the ZRA test due to high stable passive film formation due to ultra-fine grains after the ARB process.

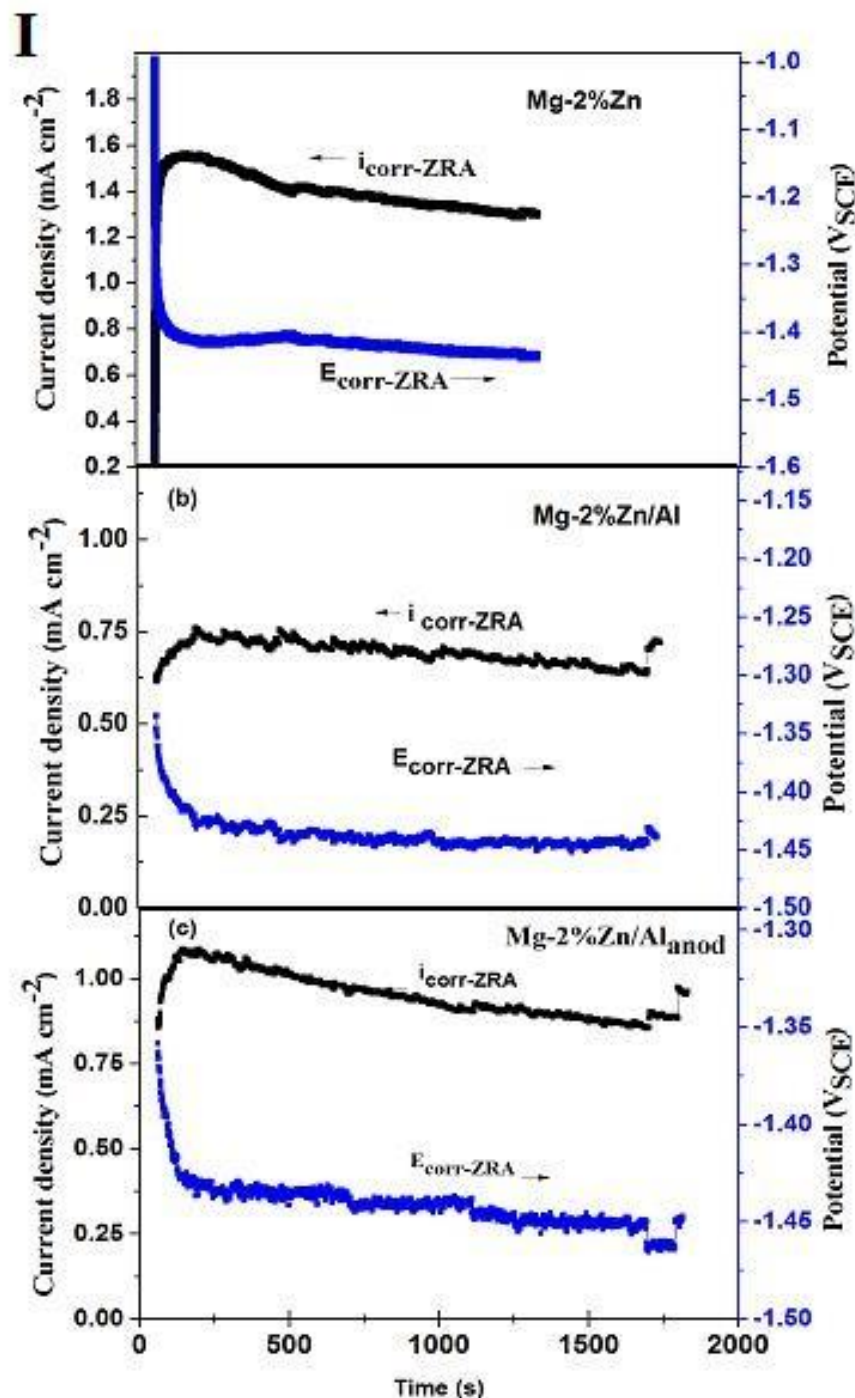


Figure 7. ZRA plots Mg-2%Zn alloys and their multilayered composites.

3.6. Immersion study.

Hydrogen evolution rate and corresponding corrosion rate of the R-1 and ARB processed multilayered composites are tabulated in Table 3. The hydrogen evolution drastically <https://materials.international/>

reduced about 1.8 times and 2.4 times in C-1 and AC-1, respectively, compared with the R-1 sample. A similar trend of corrosion rate was observed in the potentiodynamic polarization (Table 2) and immersion tests (Table 3) in 0.1 M NaCl solution. The degradation of the C-1 composites is slower than R-1 due to refined microstructure and the presence of β phases ($\text{Al}_{12}\text{Mg}_{17}$ and $\text{AlMg}_4\text{Zn}_{11}$). Further, the AC-1 samples showed less hydrogen evolution than C-1 samples due to the presence of alumina (due to anodization before the ARB process).

Table 3. Immersion test results.

Materials	V_H ($\text{ml}/\text{cm}^2/\text{d}$)	P_H (mm/y)
R-1	1.15	2.55
C-1	0.75	1.40
AC-1	0.56	1.05

4. Conclusions

The multilayered composites of C-1 and AC-1 samples were developed successfully with an average grain size in the range of 700-750 nm. Corrosion current density (i_{corr}), cathodic kinetic (β_C), passive current density (i_{pass}), and hydrogen evolution have been significantly reduced for C-1 and AC-1 samples as compared to R-1 samples. The hydrogen evolution of the AC-1 samples reduced about 2.4 times compared with R-1 samples. The stability of the passive film was evaluated by the zero resistance ammetry, which revealed that the induction time taken for passive film breakdown got increased and i_{corr} -ZRA decreased in multilayered composites. Formation of $\text{Al}_{17}\text{Mg}_{12}$, $\text{AlMg}_4\text{Zn}_{11}$ during ARB process, Al_2O_3 by anodization and passivation enhanced the corrosion resistance of the AC-1 samples.

Funding

This research received no external funding

Acknowledgments

The authors are thankful to the Mechanical Engineering department at the National Institute of Technology Karnataka, Suratkal, for providing the support in carrying out the present research work.

Conflict of interests

The authors declare no conflict of interest.

References

1. Song, D.; Ma, A.B.; Jiang, J.H.; Lin, P.H.; Yang, D.H.; Fan, J.F. Corrosion behaviour of bulk ultra-fine grained AZ91D magnesium alloy fabricated by equal-channel angular pressing. *Corros. Sci.* **2011**, *53*, 362-373, <https://doi.org/10.1016/j.corsci.2010.09.044>.
2. Clow, B.B. Magnesium industry overview. *Advanced materials & processes* **1996**, *150*, 33-35.
3. Ramesh, S.; Anne, G.; Nayaka, H. S.; Sahu, S.; Ramesh, M. R. Influence of multidirectional forging on microstructural, mechanical, and corrosion behavior of Mg-Zn alloy. *Journal of Materials Engineering and Performance* **2019**, *28*, 2053-2062.
4. Luo, A.A. Recent Magnesium Alloy Development for Automotive Powertrain Applications. *Mater. Sci. Forum* **2003**, *419-422*, 57-66, <https://doi.org/10.4028/www.scientific.net/MSF.419-422.57>.
5. Song, G.L.; Atrens, A. Corrosion Mechanisms of Magnesium Alloys. *Adv. Eng. Mater.* **1999**, *1*, 11-33, [https://doi.org/10.1002/\(SICI\)1527-2648\(199909\)1:1<11::AID-ADEM11>3.0.CO;2-N](https://doi.org/10.1002/(SICI)1527-2648(199909)1:1<11::AID-ADEM11>3.0.CO;2-N).

6. Azushima, A.; Kopp, R.; Korhonen, A.; Yang, D.Y.; Micari, F.; Lahoti, G.D.; Groche, P.; Yanagimoto, J.; Tsuji, N.; Rosochowski, A.; et al. Severe plastic deformation (SPD) processes for metals. *CIRP Annals* **2008**, *57*, 716-735, <https://doi.org/10.1016/j.cirp.2008.09.005>.
7. Toth, L.S.; Gu, C. Ultrafine-grain metals by severe plastic deformation. *Mater. Charact.* **2014**, *92*, 1-14, <https://doi.org/10.1016/j.matchar.2014.02.003>.
8. Jinfeng, D.; Guangsheng, H.; Yanchun, Z.; Bei, W. Electrochemical Performance of AZ31 Magnesium Alloy under Different Processing Conditions. *Rare Metal Materials and Engineering* **2014**, *43*, 316-321, [https://doi.org/10.1016/S1875-5372\(14\)60066-7](https://doi.org/10.1016/S1875-5372(14)60066-7).
9. Song, G.-L.; Xu, Z. The surface, microstructure and corrosion of magnesium alloy AZ31 sheet. *Electrochim. Acta* **2010**, *55*, 4148-4161, <https://doi.org/10.1016/j.electacta.2010.02.068>.
10. Wang, L.; Shinohara, T.; Zhang, B.-P. XPS study of the surface chemistry on AZ31 and AZ91 magnesium alloys in dilute NaCl solution. *Appl. Surf. Sci.* **2010**, *256*, 5807-5812, <https://doi.org/10.1016/j.apsusc.2010.02.058>.
11. Walter, R.; Kannan, M.B. Influence of surface roughness on the corrosion behaviour of magnesium alloy. *Materials & Design* **2011**, *32*, 2350-2354, <https://doi.org/10.1016/j.matdes.2010.12.016>.
12. Aung, N.N.; Zhou, W. Effect of grain size and twins on corrosion behaviour of AZ31B magnesium alloy. *Corros. Sci.* **2010**, *52*, 589-594, <https://doi.org/10.1016/j.corsci.2009.10.018>.
13. Zhang, T.; Li, Y.; Wang, F. Roles of β phase in the corrosion process of AZ91D magnesium alloy. *Corros. Sci.* **2006**, *48*, 1249-1264, <https://doi.org/10.1016/j.corsci.2005.05.011>.
14. Jamaati, R.; Toroghinejad, M.R. High-strength and highly-uniform composite produced by anodizing and accumulative roll bonding processes. *Materials & Design* **2010**, *31*, 4816-4822, <https://doi.org/10.1016/j.matdes.2010.04.048>.
15. Shi, Z.; Liu, M.; Atrens, A. Measurement of the corrosion rate of magnesium alloys using Tafel extrapolation. *Corros. Sci.* **2010**, *52*, 579-588, <https://doi.org/10.1016/j.corsci.2009.10.016>.
16. Zhang, S.; Zhang, X.; Zhao, C.; Li, J.; Song, Y.; Xie, C.; Tao, H.; Zhang, Y.; He, Y.; Jiang, Y.; et al. Research on an Mg-Zn alloy as a degradable biomaterial. *Acta Biomater.* **2010**, *6*, 626-640, <https://doi.org/10.1016/j.actbio.2009.06.028>.
17. Chen, Y.-j.; Wang, Q.-d.; Lin, J.-b.; Liu, M.-p.; Hjelen, J.; Roven, H.J. Grain refinement of magnesium alloys processed by severe plastic deformation. *Transactions of Nonferrous Metals Society of China* **2014**, *24*, 3747-3754, [https://doi.org/10.1016/S1003-6326\(14\)63528-7](https://doi.org/10.1016/S1003-6326(14)63528-7).
18. Liu, C.Y.; Jing, R.; Wang, Q.; Zhang, B.; Jia, Y.Z.; Ma, M.Z.; Liu, R.P. Fabrication of Al/Al₃Mg₂ composite by vacuum annealing and accumulative roll-bonding process. *Materials Science and Engineering: A* **2012**, *558*, 510-516, <https://doi.org/10.1016/j.msea.2012.08.037>.
19. R.J. Hebert, J.H. Perepezko: *Scr. Mater.* **50** (2004) 807–812.
20. Zarebidaki, A.; Mahmoudikohani, H.; Aboutalebi, M.-R. Microstructure and corrosion behavior of electrodeposited nano-crystalline nickel coating on AZ91 Mg alloy. *J. Alloys Compd.* **2014**, *615*, 825-830, <https://doi.org/10.1016/j.jallcom.2014.07.046>.
21. Pardo, A.; Merino, M.C.; Coy, A.E.; Arrabal, R.; Viejo, F.; Matykina, E. Corrosion behaviour of magnesium/aluminium alloys in 3.5wt.% NaCl. *Corros. Sci.* **2008**, *50*, 823-834, <https://doi.org/10.1016/j.corsci.2007.11.005>.
22. Zhao, M.-C.; Liu, M.; Song, G.; Atrens, A. Influence of the β -phase morphology on the corrosion of the Mg alloy AZ91. *Corros. Sci.* **2008**, *50*, 1939-1953, <https://doi.org/10.1016/j.corsci.2008.04.010>.
23. Bakkar, A.; Neubert, V. Corrosion characterisation of alumina–magnesium metal matrix composites. *Corros. Sci.* **2007**, *49*, 1110-1130, <https://doi.org/10.1016/j.corsci.2006.07.002>.
24. Brace, A.W. The technology of anodizing aluminium. **2000**.
25. Jilani, O.; Njah, N.; Ponthiaux, P. Corrosion properties of anodized aluminum: Effects of equal channel angular pressing prior to anodization. *Corros. Sci.* **2014**, *89*, 163-170, <https://doi.org/10.1016/j.corsci.2014.08.020>.